Preprint of **Experiments in Fluids 35 (2003) 240-251**
(DOI10.1007/s00348-003-0624-y)

Characteristics of a hot-wire microsensor for time-dependent wall shear stress measurements

Lennart Löfdahl[1], Valery Chernoray[1], Sjoerd Haasl[2], Göran Stemme[2], Mihir Sen[3]

[1] Thermo and Fluid Dynamics, Chalmers University of Technology, 41296 Göteborg, Sweden
[2] Royal Institute of Technology, Department of Signals, Sensors and Systems, Microsystem Technology, 10044 Stockholm, Sweden
[3] Department of Aerospace and Mechanical Engineering, University of Notre Dame, Notre Dame, IN 46556, U.S.A.

Received: 31 May 2002 / Revised version: 23 February 2003

Abstract Hot-wire microsensors for the purpose of measuring the instantaneous velocity gradient close to a wall have been designed and their characteristics are evaluated. The sensors were made using MEMS (micro-electromechanical systems) technology, which permits the fabrication of various micro geometrical configurations with high precision and good repeatability. The design is based on estimates of the heat rates from the sensor wire to the air, through the supports, and to the wall. Several hot-wire configurations were fabricated with wires positioned in the range of 50–250 μm from the wall. Requirements for the design and details of the fabrication methodology are outlined. The hot-wire microsensors were calibrated and tested in a flat-plate boundary layer with and without pressure gradient and were found to have good steady-state characteristics. In addition, the developed sensors were used for preliminary studies of transitional phenomena and turbulence, and the sensors were found to have good time-dependent response as well.

Nomenclature

a	diameter (m)
A	area (m^2)
d	distance to wall (m)
d_s	distance from hot-wire to wall and support length (m)
E	output voltage from anemometer (V)
h	convective heat transfer coefficient (W/m^2 K)
I	electrical current (A)
k	thermal conductivity of metal (W/m K)
k_a	thermal conductivity of air (W/m K)
l	length (m)
Nu	Nusselt number
P	perimeter (m)
Q	heat rate (W)
Q_{gen}	rate of heat generation by current (W)
Q_r	radiative heat rate (W)
R	electrical resistance (Ω)
Re	Reynolds number
S_θ	sensor temperature sensitivity (mV Pa^{-1})
S_τ	sensor wall shear stress sensitivity (mV °C^{-1})
T	temperature (°C)
T_∞	temperature of wall and surroundings (°C)
U	local fluid velocity (m/s)
U_∞	velocity outside boundary layer (m/s)
y	coordinate normal to wall (m)

Greek symbols

α_{20}	temperature coefficient of resistivity at 20°C (°C^{-1})
δ^{**}	boundary layer displacement thickness (m)
$\Delta\tau_0$	measurement error of wall shear stress (N/m^2)
ϵ	emissivity
θ	temperature fluctuation of T_∞ (°C)
ν	kinematic viscosity of air (m^2/s)
ξ	local coordinate along wire and support (m)
ρ	density of air (kg/m^3)
σ	Stefan-Boltzmann constant (W/K^{4}m^2)
τ_0	shear stress at wall (N/m^2)
τ_e	effective wall shear stress with wall influence (N/m^2)
χ	resistivity (Ω m)

Subscripts and superscripts

air	air
s	sensor support
w	sensor wire
$wall$	wall

1 Introduction

For flow control purposes, wall shear stress is an essential quantity to compute and measure. In a turbulent flow the time-averaged values of this quantity are indicative of the global state of the flow along a surface, while the time-resolved part is a measure of the unsteady structures of the flow field, which are responsible for the

individual momentum transfer events in the boundary layer. Different methods for the measurement of wall shear stresses have been developed, and most of them rely on the premise that the mean velocity gradient is proportional to the heat transfer rate at the wall. Numerous experiments have been conducted on this basis, and review papers by Winter (1977), Haritonidis (1989), Hanratty and Campbell (1996) and more recently by Löfdahl and Gad-el-Hak (1999) point out that the success of these efforts depends basically on the complexity of the flow, the geometry of the solid boundaries, and the limitations of the measuring technique used. A general conclusion to be made is that our knowledge of the wall shear stress, and in particular its fluctuating or time-resolved component, is limited.

A clear trend in all wall shear stress measurements, since the mid-1950s, is that the sensors used have smaller and smaller active sensor areas in order to improve the resolution. In this process, MEMS (microelectromechanical systems) fabrication technology has played a central role in recent years. A survey of the methods of wall shear stress measurements (Löfdahl and Gad-el-Hak 1999) shows that this technology is most suitable for instruments working on either the floating-element mechanical or thermal anemometry principles. For the current purposes only the latter method is of interest.

A thermal flush-mounted hot film sensor relies on the principle that the heat transfer from a sufficiently small heated surface depends only on the flow characteristics in the viscous region of the boundary layer adjacent to the heated region. The sensor normally consists of a thin metallic film placed on a substrate, and an electric current is passed through this film to maintain it at a constant temperature as heat is continuously transferred from the film to the moving fluid. For certain laminar flows, an algebraic relation between the local shear stress and the heat rate from the sensor can be derived, Ludwieg (1950), Liepmann and Skinner (1950) and Bellhouse and Schultz (1966). For turbulent flows, however, this relation is not valid, since there is an unknown leakage heat flow that goes through the substrate back into the fluid. This yields an effective sensor area, which is instantaneously changing and it is also significantly larger than the electrically heated part of sensor. This problem has been pointed out by many researchers, Blackwelder (1981), Haritonidis (1989), Löfdahl and Gad-el-Hak (1999), and more recently by Stein et al. (2002). Attempts have been made to insulate the sensor carefully from the substrate, for instance, by a vacuum chamber (Huang et al. 1996); however, this requires an extremely thin diaphragm to minimize the heat flow parallel to the wall. An alternative approach is to use hot-wire sensors that are mounted on the wall at a small distance from it. Schematic diagrams of such wall-mounted single or multiple hot-wires are shown in Fig. 1. This sensor design circumvents the use of the above mentioned shear stress-heat rate relation, and instead employs direct measurement of the instantaneous velocity gradient normal to the wall. This approach does not eliminate the leakage heat flow, however it reduce this heat flow to a known and controllable quantity.

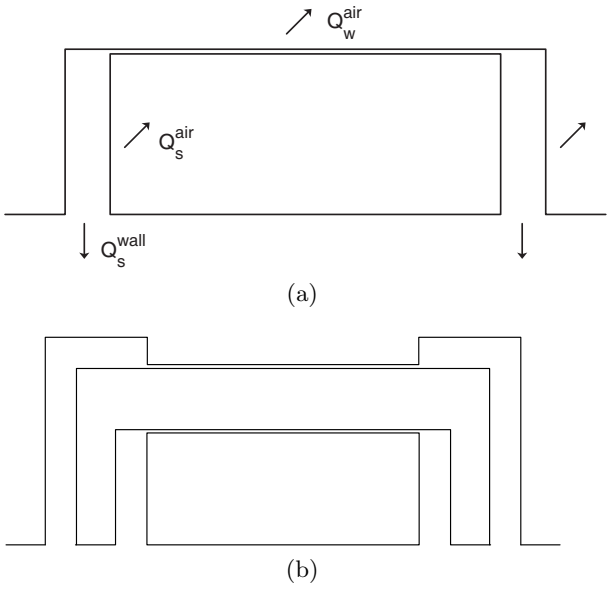

Fig. 1 Schematic of microsensors: (a) Single wire. (b) Double-wire rake.

Wall-mounted conventional hot-wire sensors for wall shear stress measurements have been used earlier by researchers such as Alfredsson et al. (1988), Wagner (1991), Nagano and Tsuji (1994), Chew et al. (1994), Fernholz et al. (1996) and Khoo et al. (2000), but in none of these investigations was MEMS fabrication technology used to produce the sensors. In the sensors described here, the advantages of MEMS, i.e. miniaturization and exact fabrication of closely spaced wires, have been used. Compared to conventional hot-wire probes, these microsensors disturb the flow less due to smaller achieved size of prongs, and in addition they are located at a fixed, prescribed, and measured distance from the wall with an a priori exactly known geometry. Very early MEMS-based wall shear stress sensors were Kälvesten (1996) and Kälvesten et al. (1996), who used a flush-mounted polysilicon piezoresistor as the heated sensitive part with dimensions $300\times60\times30$ μm^3. A more conventional flush-mounted hot film sensor was presented by Jiang et al. (1994) and Huang et al. (1996), who made single as well as arrays of flush mounted wall shear stress sensors. Their sensors consisted of a diaphragm with a thickness of 1.2 μm and a side length of typically 200 μm. The polysilicon resistor wire was located on this diaphragm, and below the diaphragm was a 2 μm deep vacuum cavity in order to minimize the heat conduction loss to the substrate. For more detailed information on MEMS wall shear stress sensors, reference can be made to the review of Löfdahl and Gad-el-Hak (1999).

The objective of the current work is to design, fabricate, and evaluate MEMS-based sensors for the measurement of local time-resolved wall shear stress. For this purpose, various configurations of wall-mounted microsensor rakes consisting of 2–10 hot-wires have been fabricated and calibrated. In the following sections the heat transfer rates from the wires are estimated, the sensor fabrication is reviewed, the necessary calibrations are discussed, and some wind tunnel test measurements are reported.

2 Estimate of heat rates

In the design of a microsensor with multiple hot-wires or a microsensor rake, estimates of the heat rates due to the various physical processes for the actual dimensions and material properties are necessary. In general, the behavior of a near-wall thermal sensor can not be predicted exactly either numerically or theoretically. However, a certain analysis, with some simplifications, of the near wall hot-wire is essential in the design of the microsensor. The estimates used are basically the same expressions as found in Comte-Bellot (1976), Perry (1982), and Bruun (1995) however, here these equations are restricted to the geometry of the current sensor. The single-wire wall-mounted microsensor is schematically depicted in Fig. 1(a). In the following analysis it is assumed that the flow and temperature fields are steady, and that the wire operates in the constant temperature mode. The mean wire temperature is T_w, and the surroundings, including the air and the wall, are at T_∞.

In the radiative heat transfer estimate, the actual sensor wire and supports were represented as heated cylinders. Then the radiative heat transfer from a heated cylinder of length l and perimeter P to the surroundings was calculated using the equation:

$$Q_r = \epsilon P l \sigma \left(T^4 - T_\infty^4\right). \tag{1}$$

where ϵ is the emissivity, σ is the Stefan-Boltzmann constant, and T is its temperature. Using this approach it was found that the radiative heat rates from the wire and supports give values about two orders of magnitude smaller than the smallest of the other heat rates calculated. Hence, the radiation effects are not considered significant.

Since the wire temperature is constant in time, the heat generated by the current through the sensor, Q_{gen}, goes convectively from the wire and its supports to the air Q_w^{air} and Q_s^{air}, respectively, and via conduction from the supports to the wall, Q_s^{wall}, as indicated in Fig. 1(a). Hence, the heat balance equation is

$$Q_{gen} = Q_w^{air} + Q_s^{air} + Q_s^{wall}. \tag{2}$$

It is noteworthy that a fraction of the convective heat is transferred to the wall, as discussed later in this section. For the present MEMS sensors, the wire and supports used are made of 2-μm thick aluminium layers, and though the supports are additionally strengthened by a material that acts as a thermal insulator this will be neglected in the heat rate calculations. Other important dimensions of the current sensor are the wire length of 400 μm, and its 2×2 μm^2 square cross section, as well as the width of the supports of 20 μm.

The heat transfer rate to the air from an infinitesimal element of the wire and support can be estimated using relationship for a two-dimensional cylinder, as can be found in the aforementioned textbooks. The King's law modification derived empirically by Kramers (1946) gives a satisfactory precision for the low Reynolds number flows. For air this may be expressed

$$Nu = 0.39 + 0.47 Re^{1/2}, \tag{3}$$

where Nu and Re are the Nusselt and Reynolds numbers, respectively, which are defined as $Nu = ha/k_a$, $Re = Ua/\nu$, where h is the convective heat transfer coefficient, a is the diameter of the cylinder, and k_a is the thermal conductivity of the fluid. Since the actual wire and supports do not have circular cross sections, the side of the square wire (2 μm) and the width of the support (20 μm) were used instead of the diameter to compute Nu and Re. It has been shown (F. Carlsson and L. Löfdahl, private communication, 2003) that this assumption is satisfactory for low Reynolds number and a moderate yaw angle.

The microsensors are designed to be located close to the wall within the viscous sublayer where the velocity profile is linear. Using Newton's viscosity law (Panton 1996), a relation between wall shear stress and the velocity gradient may be written:

$$\tau_0 = \rho\nu \left(\frac{\partial U}{\partial y}\right)_{y=0} = \rho\nu \frac{U}{d}, \tag{4}$$

where U is the local flow velocity, and d is the distance to the wall.

As the wire is brought closer to the wall, there are two effects that alter the convective heat rate: the streamline pattern is altered and the temperature boundary condition is changed due to the presence of the wall. For a given fluid, as shown by many investigators (Janke 1987; Khoo et al. 1996; Chew, Khoo and Li (1998); Lange et al. 1999), the type of wall material and the distance to the wall are most significant in the determination of the wall influence. A common practice is to take the effect of the wall into account by introducing some "effective" fluid velocity near the wall in the King's law instead of the actual velocity. Unfortunately, no universal wall correction can be obtained (see discussion in Chew, Khoo and Li 1998), so approximate corrections of the wall influence have been derived for perfectly conductive and perfectly insulating walls. The silicon substrate placed under the current MEMS sensor has a thermal conductivity of about 6000 times that of air, and hence can, with very good accuracy be treated as perfectly conductive. The

correction for the case of a perfectly conductive wall was proposed by Lange et al. (1999) and can be rewritten in terms of wall shear stress in the following way:

$$\tau_e = \tau_0 \left[1.0 - \exp\left(-0.4\frac{\tau_0 d^2}{\rho\nu^2}\right)\right]^{-1}. \quad (5)$$

This expression was derived using numerical simulations performed for an infinite 5-μm diameter circular cylinder in air heated to a temperature range 21–100°C and assumes that the wire is located in the viscous sublayer. The wall influence on the heat transfer is given as a relationship between the effective wall shear stress τ_e and the actual wall shear stress τ_0. The hot-wire is located at a distance d from the wall, and ρ and ν are the density and the kinematic viscosity of the fluid, respectively. Hence, in order to take into account the wall influence in estimations described further on, the actual wall shear stress τ_0 will be replaced by τ_e according to Eq. (5).

For an infinitesimal element of the sensor, the heat generated by an electrical current I is balanced by the heat convected into the air and by conduction, so that heat balance equation is

$$kA\frac{d^2T}{d\xi^2} - hP\,(T - T_\infty) + \frac{I^2\chi}{A} = 0. \quad (6)$$

Here A is the local cross-sectional area, and P is the local perimeter of the infinitesimal element. These quantities are different for the wire and the supports, and thus are functions of the coordinate defined along the sensor ξ. The resistivity of the material χ is assumed to be linearly dependent on temperature, as $\chi = \chi_{20}[1+\alpha_{20}\,(T - T_{20})]$, and the heat transfer coefficient h with incorporated wall effects may be obtained from Eqs. (3) and (5)

$$h = \frac{k_a}{a}\{0.39+0.47\left(\frac{\tau_0 da}{\rho\nu^2}\right)^{1/2}\left[1.0 - \exp\left(-0.4\frac{\tau_0 d^2}{\rho\nu^2}\right)\right]^{-1/2}\}, \quad (7)$$

where d now is the distance from the treated infinitesimal element of sensor to the wall. Thus, in Eq. (6) P, A, and h are functions of the coordinate ξ, and the temperature $T(\xi)$ is the unknown quantity. A constant-temperature anemometer adjusts the current to keep the electrical resistance of the sensor constant, and both the resistance of the wire and that of the supports are temperature dependent so that the total resistance is constant:

$$R_w + 2R_s = \text{const}, \quad (8)$$

where R_w and R_s are the resistances of the wire and one support, respectively. The boundary conditions on the temperature are its value at the wall $T = T_\infty$ and the symmetry condition at the center of the wire $dT/d\xi = 0$.

Eq. (6), together with Eqs. (7), (8) and the boundary conditions, is a linear differential equation with variable coefficients that can be numerically solved, and the solution gives the temperature distribution along the wire and the supports. This has been done using the commercially available software package Matlab (The Mathworks, USA), and an example of the temperature distribution is shown in Fig. 2. In this figure, the temperature distribution along the wire and the supports of microsensor is shown for a 400 μm long wire and 100 μm long supports. It should be noted that the temperature is changing along the supports, because they are of finite size and not massive. Using the above-derived expressions it is now possible to explore the thermal characteristics of the sensor by varying the wire overheat, support length, and wall shear stress, as discussed in the next section.

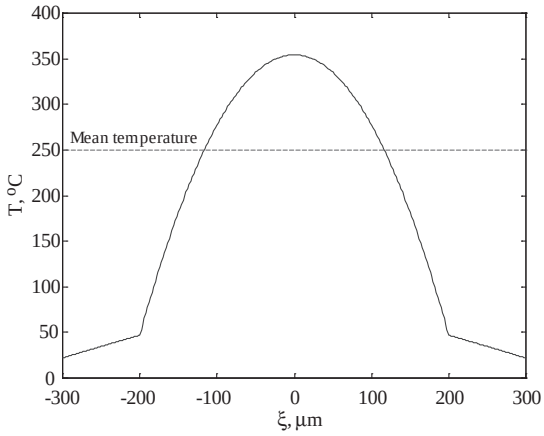

Fig. 2 Temperature distribution along wire and supports of microsensor. Wire is at -200 μm$< \xi < 200$ μm, and remainder is supports. Note nonuniform temperature distribution along the supports since they are not massive.

3 Thermal characteristics of sensor

The different terms of Eq. (2) may be expressed as follows: heat convected to the air from the wire

$$Q_w^{air} = hP_w \int_{l_w} (T - T_\infty)\,\mathrm{d}\xi \quad (9)$$

and from the two supports

$$Q_s^{air} = 2P_s \int_{l_s} h(\xi)\,(T - T_\infty)\,\mathrm{d}\xi. \quad (10)$$

and finally the conductive heat rate from both supports to the wall

$$Q_s^{wall} = 2kA_s\left(\frac{dT}{d\xi}\right)_{\xi=0}. \quad (11)$$

The different contributions to the heat balance were estimated using the Matlab software package, and Fig. 3 shows normalized heat rates as a function the wall distance at a constant value of the wall shear stress, in this particular case $\tau_0 = 1$ Pa. In order to obtain good

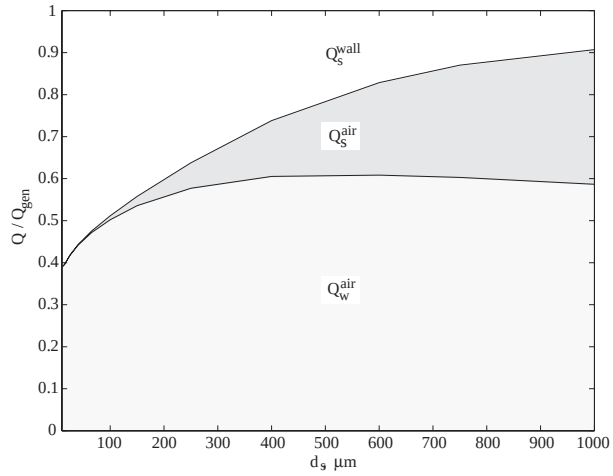

Fig. 3 Heat rates of the microsensor for different support lengths; τ_0=1 Pa.

sensitivity of the wire to the flow velocity and low sensitivity to the temperature variation, the convective heat transfer from the wire to the air Q_w^{air} should be large compared to the other terms. Figure 3 shows that for the current MEMS sensor the convective heat transfer from the wire constitutes about 50–60% of the total heat generated. According to Bruun (1995), a conventional hot wire has a corresponding value at 80–85%; however for the current wall-mounted hot wire the conduction out of the wire is larger. This is first explained by higher thermal conductivity of aluminium as compared to tungsten, and second by lower convective heat transfer because of the much lower velocity in the wall region as compared to those velocities at which conventional hot-wires are used. As for conventional wires, the relation of convection to conduction may be increased by increasing the wire length-to-diameter ratio. Additional calculations conducted revealed that the proportion of the convective heat transfer might be increased up to about 70–80% if the length-to-diameter ratio of the wire is increased up to about 400. However, it was not in the scope of the current work to make such sensors.

By looking at Fig. 3 it can be seen that a microsensor with supports longer than 200 μm will have non-negligible convective heat transfer from the supports, i.e. more than 5%, since Q_s^{air} at this distance from the wall passes the 5% threshold. Supports much longer than 200 μm can create errors since an uncontrolled velocity gradient might be formed and influence the calibration. In order to avoid such errors, only microsensors with supports less than 250-μm length were fabricated.

Computed calibration curves of the microsensor are shown in Fig. 4 for wires located 50 and 100 μm from the wall as a function of varied wall shear stress. The overheat ratio of the wires used is 1.5, and the theoretical voltage is the output from the anemometer. Solid and dashed lines show the computed calibration curves with and without wall effects, respectively, and it obvious from the figure that the sensor sensitivity is strongly influenced by the proximity of the wall. Above a certain value of the wall shear stress, the influence from the wall disappears and the microsensor wire starts to work as a conventional hot-wire. This can be expected since the influence from Eq. (5) disappears at large values of d. This occurs typically at wall shear stress values of about 400 mPa and 1500 mPa for support lengths of 100 μm and 50 μm, respectively.

For instance, for a wire located at $d_s = 100$ μm and $\tau_0 \geq 400$ mPa, the wall-mounted microsensor behaves like a conventional hot-wire with a "fast" frequency response, and for values less than 400 mPa it behaves similar to a flush-mounted conventional hot-film with an associated thermal inertia. However, as compared to a flush-mounted hot film sensor, the present microsensor has a constant rate of heat conduction from the supports to the wall through a very small area. It should be pointed out here that the same wall shear stress may also be measured by using a wire that is located closer to the wall, but with a smaller output signal since the local velocities will be smaller. As can be seen from Fig. 4, an expected value of the output signal is typically in the range of 80–150 mV/Pa. Corresponding values for a flush-mounted hot film with a vacuum cavity underneath (Huang et al. 1996) are approximately 10 mV/Pa, and without cavity about 1 mV/Pa. This demonstrates another advantage of the present microsensor, its higher sensitivity.

An analysis of the heat transfer characteristics of the microsensor shows that wires located too close to the wall will loose sensitivity because of low fluid velocity, proximity to the wall, and conduction through the supports. As a consequence, since the expected output signal from anemometer is fairly small, it is desirable to vary the distance between the wire and the wall. This situation is obtained through a microsensor rake of multiple

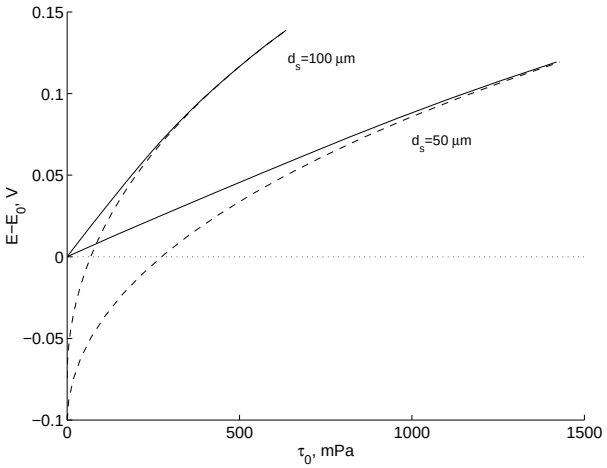

Fig. 4 Computed calibration curves with (*solid lines*) and without (*dashed lines*) wall influence. Sensor support lengths are 50 and 100 μm.

wires, where each wire is aimed to cover different ranges of the wall shear stress.

It is not necessary that wires creating the rake should be operated simultaneously, since simultaneous work of wires in the near-wall region is quite problematic due to the thermal interference that can hardly be avoided. As it was shown, for instance, by Österlund and Johansson (1995), thermal interference of two parallel wires becomes significant for Péclet numbers below 50 based on distance between the wires. Analysis shows that if the desired distance between the wires is 50 μm, then the minimal characteristic flow velocity at which the thermal interference is avoided corresponds to about 20 m/s — a velocity that hardly can be obtained in the near-wall region. An other possible interaction between the wires is aerodynamical blockage, but this effect is not so significant as can be shown. Assume that the spacing between the wires is about 25 wire diameters, and that the flow is laminar, then the streamline distortion created by one wire will not be felt by other wire if $Re_a \gtrsim 0.1$, implying that $\tau_0 \gtrsim 0.3$ Pa. Moreover, this effect will not be considered as affecting the measurements, since all aerodynamic interactions between elements of the sensor are included into the calibration.

To summarize, an analysis of the heat transfer characteristics of the microsensor shows that a good design should have short supports in order to minimize convective heat loss from supports to the air, but on the other hand, wires located too close to the wall will loose their sensitivity because of low fluid velocity, heat transfer to the wall, and conduction through the supports. Hence, the wire distance from the wall is a compromise, and it could be an advantage to have a microsensor rake of multiple wires at different distances from the wall to measure the wall shear stress in different ranges.

4 Design and fabrication

The objective of the MEMS-fabricated hot-wire sensor is to measure the instantaneous velocity gradient of the innermost part of the boundary layer. In principle, this requires only one hot-wire at a certain distance from the surface, however, to increase the flexibility of the device, several wires in a rake pattern were used. Moreover, in the design process variants where the wires form different angles with the main flow direction were fabricated in order to resolve unknown flow angles of the instantaneous velocity vector. SEM pictures of two MEMS hot-wire sensors are shown in Fig. 5: a double-wire microsensor is shown in Fig. 5(a), and a double five-wire rake is shown in Fig. 5(b).

A basic requirement of the measuring technology is that the innermost of the wires is located within the linear part of the velocity profile. For turbulent flow, the linear sublayer extends up to about five wall units, and this means that a maximum value of the shear stress, which can be measured by wire located 50 μm from the wall, will be about 2.5 Pa. This limiting value was considered as sufficient when the microsensors were designed. In the same manner, the limiting wall shear stress for a wire located 100 μm above the wall would be about 0.7 Pa. Hence, such rake of two wires will in principle cover the range of the wall shear stresses 0–2.5 Pa with reasonable accuracy.

All measurements were conducted close to a smooth surface, which means that all electrical contacts had to be either far away from the sensor on the surface, or on the "other" side of the measuring plane in order not to interfere with the flow. Putting all these requirements together, a hybrid design was chosen where the surface and the hot-wire chip were made from different silicon wafers. The surface where the measurements are conducted would just be a flat silicon wafer with one or more holes, while the hot-wire chip, shown in Fig. 6, would come from another silicon wafer where several hundred devices could be manufactured simultaneously. This allowed for a very small chip size, since no conductors in the measuring plane were needed, and the flat surface required around the hot-wires was provided by the covering wafer.

Well-tested procedures were used for the production of the sensors. Aluminum was chosen for the wire, since the temperature coefficient of resistivity of aluminum is the same as that of tungsten. The maximum operating temperature of aluminum wires, which is limited

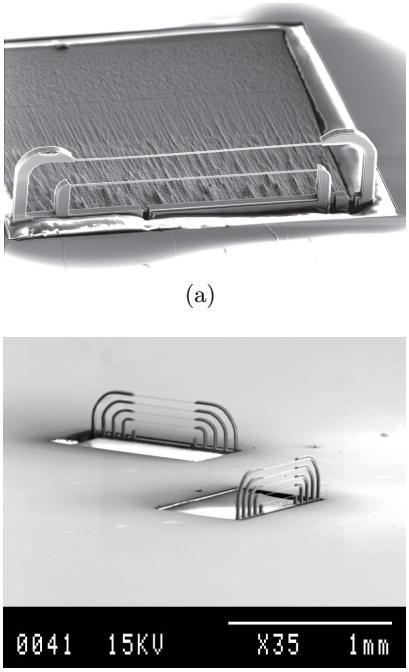

(a)

(b)

Fig. 5 SEM pictures of two fabricated MEMS hot-wire sensors: (a) Double wire microsensor. (b) Two five-wire microsensors at 90° to each other.

by its melting point, is about 660°C, giving the highest possible overheat ratio for the wires of about 2.5. The wire dimensions were selected with flow scales in mind (Löfdahl and Gad-el-Hak (1999)), and microsensors with hot-wires of length × width of 200×1, 400×2 and 600×3 μm^2, respectively, were fabricated. The wire thickness was equal to the thickness of sputtered aluminum, i.e. 2 μm, and the calculated resistance of such a wire was about 2.8 Ω, which is within the range of conventional hot-wires enabling the use of normal hot-wire electronics. The distance from the hot-wires to the surface ranged from 50 to 250 μm, where, according to calculations, the convective heat loss from the supports was negligible (Sect. 3).

A bulk micromachining process was used to make the microsensor. Production involved more then 20 distinct stages, which are described in more detail by Haasl et al. (2002). The fabrication was performed on a silicon-on-insulator wafer consisting of three layers: a 20 μm thick silicon layer, a buried 1.5 μm thick SiO_2 layer and a 525 μm thick silicon substrate. Figure 7 shows the major fabrication steps of the sensor, which briefly may be described as:

a. A layer of the oxide on the top silicon substrate was formed to define areas where the aluminium ground leads are isolated from the substrate. The thickness of the silicon oxide layer was 200 nm.
b. The aluminium pattern of the wires and leads is created from aluminium layer of 2-μm thickness. Reactive ion etching was used on this step, thus allowing well-defined edges.
c. The thick silicon substrate of the backside was etched anisotropically in an inductively coupled plasma (ICP) etch. Subsequently, the buried oxide layer of the wafer was removed.
d. Following this, the supports for the sensors were formed in an ICP etch. This resulted in 20-μm thick supports sticking out of the body of the sensor. The silicon underneath of the wire was removed in the same machine.
e. Finally, the sensors were glued to printed circuit boards, wire-bonded to them, inserted and glued to the cover chip. The cover chip used for holding the sensors was a 300-μm thick silicon plate of size 20×20 mm^2 (in the figure it is shown in reduced size). The holes in these wafers were etched in a potassium hydroxide solution, and the slanted shape of the holes eased the assembly of the sensor in the holding wafer.
f. This part of the figure shows the manufactured sensor assembly.

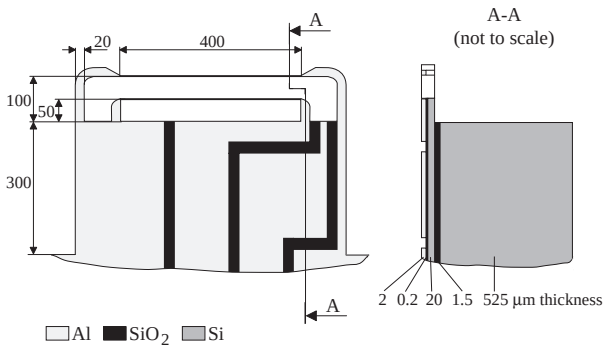

Fig. 6 Design of microchip for two-wire sensor (picture, *right* not to scale; all dimensions given in μm).

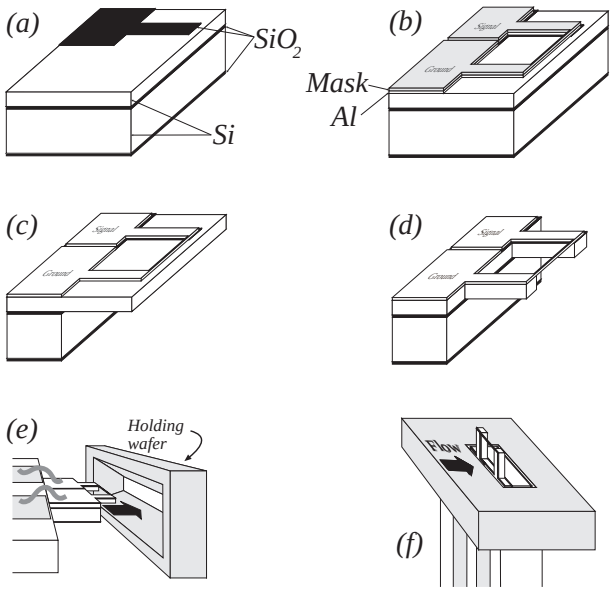

Fig. 7 Stages of manufacture of MEMS hot-wire sensor (see text).

More comprehensive description on the use of MEMS technology for sensor fabrication can be found in Löfdahl and Gad-el-Hak (1999). References to literature surveys in the MEMS field are also given in this work.

5 Wind tunnel tests

Experiments were conducted with some of the fabricated microsensors in a closed-circuit wind tunnel at Thermo and Fluid Dynamics, Chalmers University of Technology. This tunnel has a test section of 1.8-m width, 1.2-m height, and 3-m length. A free-stream turbulence level in the test section is well below $0.001U_\infty$, and the flow temperature can be controlled with a precision of ±0.1°C. The wind tunnel velocity was monitored using a Pitot–Prandtl tube connected to a digital micromanometer, which also had sensors for temperature and absolute pressure readings. The experiments were performed in boundary layers without pressure gradients, and with a slightly negative pressure gradient accomplished by using a flat plate and a wing section, respectively. During the tests the microsensors were positioned on a specially designed surface-mounted rotatable chuck on the surface of the model. Constant-temperature anemometers (Dantec) were used to monitor the sensors. All electrical connections between the sensors and the anemometer

bridge were made by coaxial cables soldered to the sensor and equipped with BNC connectors for stability and reliability of the electrical connections.

Boundary layer profiles were measured by a standard boundary layer probe (Dantec), which had a tungsten wire of 5-μm diameter and 1.5-mm length. This probe was also monitored by a constant-temperature anemometer at an overheat ratio of 1.8. The traverse mechanism used to position the probe had a precision of 1 μm in both the normal-to-the-wall y and the spanwise directions, and 5 μm in the streamwise direction. The initial distance to the wall of the hot-wire probe was measured using a high-resolution, high-magnification video camera. The output signal from the anemometers was digitized by a multichannel 16-bit analog-to-digital converter, and the data were stored for processing in a PC.

5.1 Calibration

The relation between the steady-state convective heat rate from the wire and the local velocity around it forms the basis for the static calibration. As mentioned, the wall affects convective heat rate and various aerodynamical interactions between the wires, the supports and the wall take place. Therefore, the sensor must be calibrated in situ, i.e. close to the wall, so that both the dynamic and thermal conditions during calibration will be reproduced during the measurement. Near-wall corrections (Polyakov and Shindin 1978; Zemskaya et al. 1979; Bhatia et al. 1982; Krishnamoorthy et al. 1985; Khoo et al. 1996; Janke 1987; Lange et al. 1999) need not be applied for the measurements in this case, since those corrections were developed for sensors calibrated away from the wall and then used near it. This situation does not arise in a wall-mounted microsensor since the hot-wires are at fixed distances from the wall. Nevertheless, proper wall corrections may be incorporated into the calibration as will be discussed below.

During the calibration the voltage of the CTA bridge must be related to the wall shear stress by some relationship. Calibration data points may be fitted in two different ways: by polynomial fit or by some sort of King's law. For the measurement in laminar flow the choice of relationship used is obviously not crucial, so either of these two methods can be used. In turbulent flows, on the other hand, the King's law is preferable since extrapolation is often required and polynomials tend to deviate strongly outside the calibration region (Fernholz et al. 1996). The wall effects cause the response of the wall mounted wire to deviate from the classic King's law (Sect. 3 and Fig. 4), and therefore, a modified King's law with additional terms is introduced to improve the calibration fit. A possible way of doing this is to use classic King's law with incorporated wall-correction (Wagner 1991; Warnack 1996; Fernholz et al. 1996). In the current experiment, both procedures are considered.

For the purpose of evaluating the sensors, only calibrations in a laminar boundary layer were carried out. Relatively high values of the laminar wall shear stress were obtained, since the transition was suppressed by adding a weak favorable pressure gradient. In the calibration, the aim was to obtain a relation between the microsensor output voltage and the wall shear stress, and this process was done in two main steps. In the first, the reference mean wall shear stress versus the velocity outside the boundary layer was obtained for the chosen free-stream velocity range. Then, in the second step the actual calibration in which the sensor output was related to the wall shear stress was conducted.

First, the boundary layer profiles $U(y)$ were measured at the location of the microsensor with a sufficiently small resolution in the normal direction. At least ten measured points were well-approximated near the wall by a straight line. The measured profiles were similar, and collapsed on a single plot when scaled with boundary layer variables. The displacement thickness δ^{**} was used as a length scale, and the velocity outside the boundary layer U_∞ as the velocity scale. Figure 8 shows nine measured velocity profiles in the range of free-stream velocities from 5 to 32 m/s. The straight line in this figure is a linear approximation of the near-wall slope in the scaled variables, which is the same for all measurements. From this the wall shear stress can be calculated using Newton's viscosity law

$$\tau_0 = \rho\nu \left.\frac{\partial(U/U_\infty)}{\partial(y/\delta^{**})}\right|_{wall} \frac{U_\infty}{\delta^{**}}. \tag{12}$$

The integral scales of the boundary layer, U_∞ and δ^{**}, can be measured with good accuracy, and this has a crucial impact on the accuracy of the wall shear stress measurement.

In order to obtain an analytical expression for the wall shear stress as a function of the velocity outside the boundary layer, all the measured points were plotted in one graph (Fig. 9) and approximated by a power law. From laminar boundary layer theory (Panton (1996)), the wall shear stress ($\delta^{**} \sim U_\infty^{-1/2}$) can be fitted to experimental data as

$$\tau_0 = C U_\infty^{1.5}. \tag{13}$$

In the second step the microsensor calibration curve, which is the anemometer bridge output voltage versus the wall shear stress, was obtained. For a set of velocities U_∞ the output voltage E was recorded, and using Eq. (13), the corresponding values of the wall shear stress τ_0 were computed. Experimental calibration curves for the microsensor are shown in Fig. 10, which contains two sets of data, where the crosses and dots are for the wires 50 and 100 μm above the surface, respectively. For comparison, the previous computational estimations of Fig. 4 are included in this figure. It can be noted that the experimental calibrations are slightly higher; however this

is not surprising since many of parameters included in the theoretical analysis may be different from the actual. In particular, the exact value of the overheat ratio in experiments is never known.

A fifth-order polynomial was used to fit the calibration data, which yielded an average error of less than 1%. However, for turbulent flows this curve fit has a tendency to loose its accuracy outside the calibration interval, and therefore the simple King's law was tried. Using this law without a correction for the wall influence, the average fitting error was unacceptably high (on the order of 5%), and therefore a wall correction was included, yielding

$$E^2 = A + B{\tau_e}^n. \tag{14}$$

This significantly improved the accuracy of the calibration, and the average error was decreased to the same limit as was obtained by the fifth-order polynomial fit.

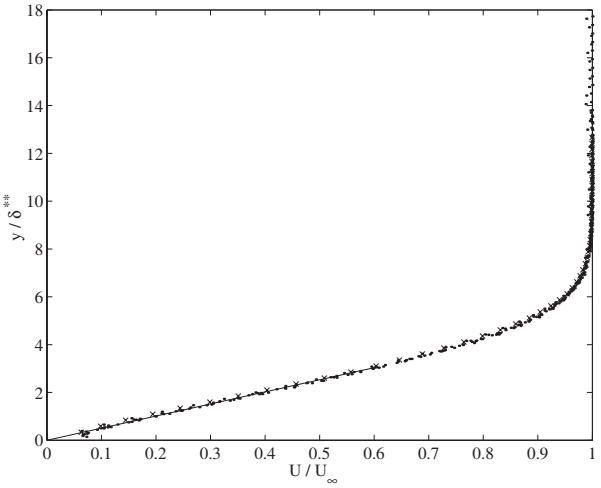

Fig. 8 Nine mean velocity profiles for different free-stream velocities. it Solid line is an approximation of the near-wall slope.

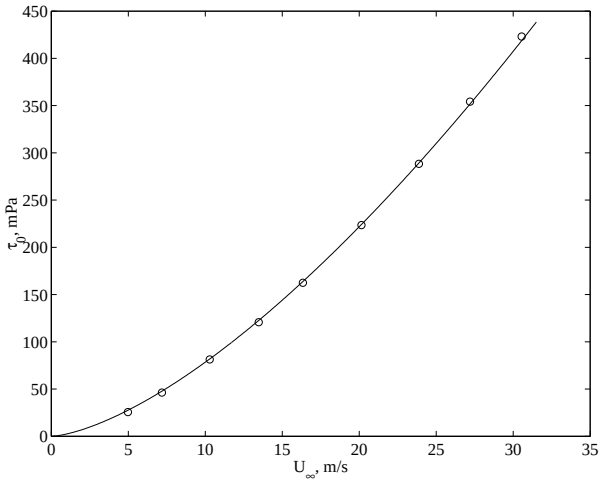

Fig. 9 Wall shear stress versus velocity outside boundary layer. *Line* is power-law approximation.

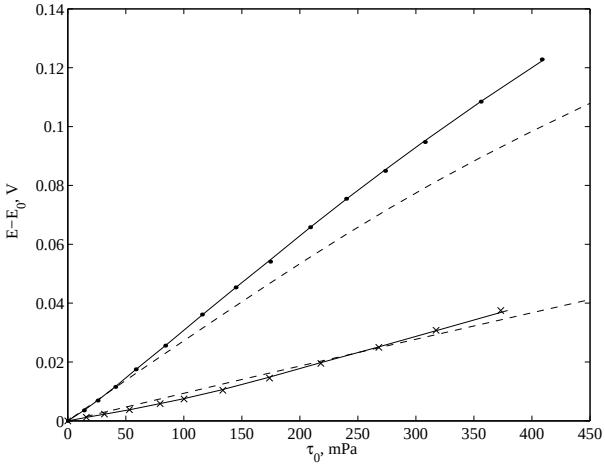

Fig. 10 MEMS sensor calibration curves. *Crosses*, wire at 50 μm from wall; dots, 100 μm; *solid lines*, King's law approximation with wall correction; *dashes*, computed calibrations.

Similar calibration procedures were used e.g. by Wagner (1991), and Warnack (1996) for near-wall hot-wires. In their works, the equation of Janke (1987) is used for τ_e, and this relationship has additional constants that take into account the specific wall material. However, the Janke expression also has the disadvantage of overshooting the wall influence at high velocities. In the case of a highly conductive wall, as in the current experiment, Eq. (5) is sufficient and preferable and no additional adjustments are required. Hence, Eq. (14) was used and the approximations are shown in Fig. 10 as solid lines, where it can be seen that the curves describe the full range of the calibrations very well.

5.2 Sensitivities

Using Eq. (14) it is possible to estimate the sensitivities of the sensor to the wall shear stress and to the temperature. Following conventional hot-wire practice (Bruun 1995), the output bridge voltage E can be decomposed as follows:

$$E^2 = (a + b{\tau_e}^n)(\overline{T} - T_\infty). \tag{15}$$

This expression yields one wall shear stress part (for conventional hot-wires it is the velocity) and one temperature sensitive part. The constants a and b are new and are not temperature dependent. Temperature $\overline{T}$ is approximately equal to the mean temperature of the sensor, and by differentiation the sensitivity factors are obtained.

$$S_\tau = \frac{\partial E}{\partial \tau_0} = \frac{nb{\tau_e}^{n-1}}{2}\left[\frac{\overline{T} - T_\infty}{a + b{\tau_e}^n}\right]^{1/2} \frac{1 - K\tau_e e^{-K\tau_0}}{1 - e^{-K\tau_0}} \tag{16}$$

$$S_\theta = \frac{\partial E}{\partial \theta} = -\frac{1}{2}\left[\frac{a + b{\tau_e}^n}{\overline{T} - T_\infty}\right]^{1/2}, \tag{17}$$

where K is given by

$$K = 0.4 d_s^2/(\rho\nu^2). \tag{18}$$

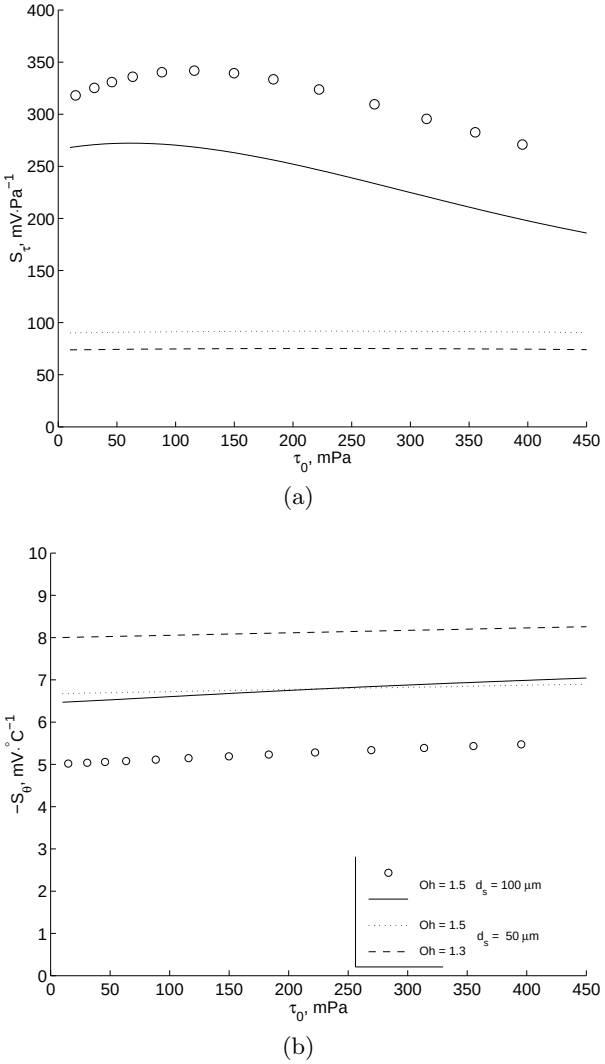

Fig. 11 Sensitivities of microsensor: (a) Sensitivity factor for wall shear stress S_τ. (b) Sensitivity factor for temperature S_θ. *Symbols* denote experiment for wire at 100 μm from the wall at overheat ratio 1.5. *Lines* represent computated values.

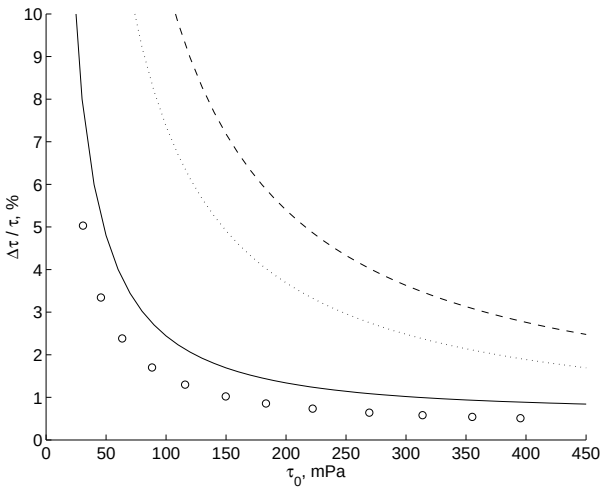

Fig. 12 Relative percentage error of wall shear stress measurement caused by temperature fluctuation of -0.1 °C. *Symbols* as in Fig. 11.

Here θ represents a small fluctuation in fluid temperature T_∞, and $\tau_e(\tau_0)$ is defined by Eq. (5). As compared to the corresponding equations for a conventional hot-wire, Eqs. (16) and (17) are expressed in τ_e and an extra term appears in the right-hand side of Eq. (16) from the wall correction of Eq. (5). According to Bruun (1995) this method of evaluating of the hot-wire probe sensitivities is one of the most accurate, and it does not require lengthy measurements as do the methods of direct velocity and temperature calibration. Moreover, the sensitivities obtained from Eqs. (16) and (17) depend very slightly on precision of temperature measurements, as can be proved by second differentiation of Eqs. (16) and (17).

Measured values of the sensitivity factors for the wall shear stress S_τ and temperature S_θ are marked with dots and are shown as function of the wall shear stress τ_0 in Fig. 11(a) and 11(b), respectively. An overheat ratio of 1.5 was used in the experiment, and measurements were made for only one wall distance d of 100 μm. For comparison, sensitivities computed from the theory of Sect. 3 and corresponding to the experiment are included in Fig. 11(a) and 11(b) as well. These data are obtained directly, through the virtual calibration at number of ambient temperatures. In addition, two cases of different overheats for the wire 50 μm from the wall are included. Looking at Fig. 11(a) it can be seen that for the wall distance d_s=50 μm, the sensitivity increases with increasing overheat ratio. Hence, higher overheat ratios are preferred for the measurement of wall shear stress fluctuations. From this figure it may also be noted that the sensitivity in the wall shear stress measurements increases as the distance from the wire wall increases. The sensitivity of the wire at d_s=100 μm is about two to three times as high as that for the wire at d_s=50 μm. The reason for this is twofold: the gradient is resolved better, and the influence from the wall is reduced. Focusing the attention on d_s=100 μm, it is obvious that S_τ is reduced as the wall shear stress is increased. This is mainly a consequence of Eq. 7, and this expression for the heat transfer coefficient also explains the almost constant values of S_τ for d_s=50 μm. Noteworthy in Fig. 11(a) is also that the difference between the experimentally determined values of S_τ and the theoretical, for d_s=100 μm is of the same magnitude as corresponding data in the sensor calibration, shown in Fig. 10. Looking at the temperature sensitivities shown in Fig. 11(b), it is apparent that the lower overheat ratio yields a higher sensitivity, S_θ. This is clearly depicted for d_s=50 μm and is explained by Eq. 17. The same observations are valid for conventional hot-wires (Bruun 1995). The difference between the measured and computed sensitivity factors for d_s=100 μm is about the same as for S_τ.

An important parameter that can be derived from the sensitivities is the relative error of the wall shear stress measurement due to uncontrolled temperature fluctuations defined as

$$\frac{\Delta\tau_0}{\tau_0} = \frac{1}{\tau_0}\frac{S_\theta}{S_\tau}\theta. \qquad (19)$$

This relative error tends to infinity as the wall shear stress decreases towards zero if θ is finite. For the experimental facility used, this error can be estimated if a range of temperature variation is known. For instance, if the flow temperature is kept constant within $\pm 0.1^\circ$C, as in the wind tunnel used, then for a temperature fluctuation of $\theta = -0.1$ °C the relative wall shear stress measurement error can be obtained as shown in Fig. 12. For a temperature fluctuation with positive sign, the error will have a correspondingly negative sign. Assuming that the relevant measurement accuracy is $\pm 5\%$, from this figure it can be concluded that the sensor located 50 μm from the wall can be used for the measurement of the wall shear stress values higher than about 200 mPa at an overheat ratio of 1.3, and higher than about 150 mPa at an overheat ratio of 1.5. To measure lower values of the wall shear stress, the wire located 100 μm from the wall, which gives a reasonable accuracy of about 50 and 40 mPa at overheats of 1.3 and 1.5 respectively, should be used. The bottom line of this is that at lower values of the wall shear stress, care should be taken to control the temperature with better precision or temperature compensation of measurements by electronic or data correction should be used. It should be noted that the value of the relative error

$$\frac{\Delta\tau_0}{\tau_0} \to -\frac{\theta}{n(\overline{T} - T_\infty)} \qquad \text{as} \qquad \tau_0 \to \infty. \qquad (20)$$

This relative error is finite even at infinitely large values of the wall shear stress.

5.3 Time-resolved measurements

The possibility to perform time resolved wall shear stress measurements was a main objective in designing the current hot-wire microsensor. As a first practical application, the ability of the designed MEMS sensor to detect some phenomena, events in the laminar-turbulent transition process is demonstrated. For this purpose the laminar flow breakdown was artificially triggered using the same model as was used for the sensor calibration. To provoke the flow breakdown, disturbance is introduced in an initially laminar boundary layer by localized periodic blowing and suction through a hole located about 80 mm upstream of the microsensor. Frequency of the artificial disturbance was fixed at 260 Hz, and in Fig. 13 measured by microsensor velocity traces are shown for three different values of the free stream velocity. To obtain these measurements, the recorded instantaneous voltages were converted to velocities and ensemble averaged over 25 realizations. In the figure, four periods of obtained transitional flow traces are shown, and it is clearly visible how the disturbance in the boundary layer grows and how the transition is promoted as flow Reynolds number increases. Initially the sinusoidal disturbance starts to loose its periodicity, then it is distorted by appearing at higher harmonics and getting more and more random. It is worthwhile to note that the amplitude of the instability wave at 13 m/s was fairly small, about 0.5% of the free stream velocity. To our knowledge this is the first experiment where MEMS-based wall-mounted sensor was able to register weak eigen-disturbances of the boundary layer during the transition process.

In time-resolved measurements, the issue of the dynamic response of the sensor must be considered. The response of thermal sensors to high-frequency fluctuations

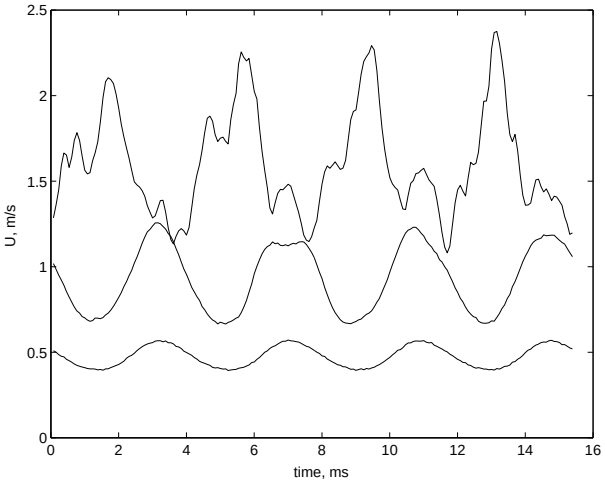

Fig. 13 Velocity traces of laminar-turbulent transition measured by MEMS sensor. Free-stream velocity 13, 20 and 24 m/s (from *bottom* to *top*).

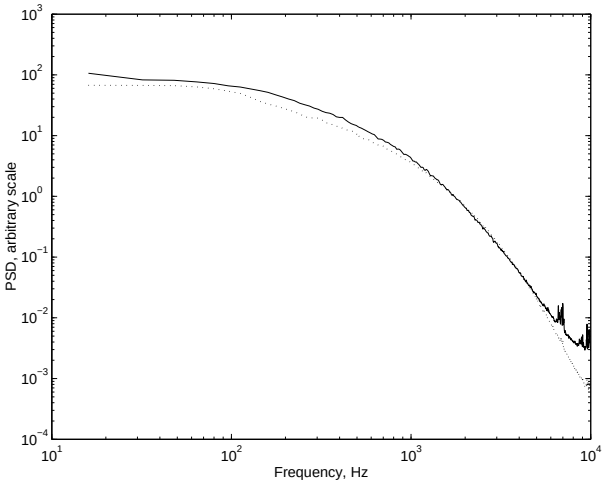

Fig. 14 Power spectral density measured with MEMS sensor (*solid line*) and with conventional hot-wire (*dotted line*) in turbulent boundary layer.

has long been considered as a limitation, Hinze (1975), Bradshaw (1971), Comte-Bellot (1976), Perry (1982). In this perspective the present MEMS sensor is no different from an ordinary hot-wire when used for relatively high wall shear stress where the wall influence disappears. For low wall shear stress, the signals obtained from high-intensity and high-frequency fluctuations are somewhat distorted by the nonlinear nature of the interaction between the fluid dynamics and the temperature field. Recent studies of this have been made by Khoo et al. (1998), Chew, Khoo, Lim and Teo (1998), Khoo et al. (1999) and Teo et al. (2001). Furthermore, in turbulent flows the additional problem of an imperfect spatial resolution arises, since a hot-wire attenuates the measured velocity fluctuation if that fluctuation occurs over a length-scale smaller than the sensing length of the wire. The effect of hot-wire length on the spatial resolution has been studied by Ligrani and Bradshaw (1987), Alfredsson et al. (1988) and Khoo et al. (1997). To evaluate the frequency response of the current microsensors simply, a spectrum of fluctuations in a fully turbulent boundary layer was measured. In Fig. 14 comparison of two spectra, one measured by a conventional hot-wire and the other by a microsensor, are shown. Since the MEMS calibration do not extend to high values of the wall shear stress, which are present in turbulent flow, the spectra are represented in an arbitrary scale. The two spectra demonstrate almost the same shape, except for small spikes in the spectrum obtained by MEMS sensor at frequencies higher 6 kHz. Most probably this is due to the noise within electrical circuits. So it may be concluded that for frequencies less than 5 kHz, the MEMS sensor reveal a similar dynamic response as a conventional hot-wire.

6 Concluding remarks

MEMS-based sensors for wall shear measurements were developed and studied in detail. The devices were based on heat transfer calculations and were analyzed from this perspective. Sensors of different configurations and multiple wires for diverse applications were manufactured using MEMS technology. The sensors were calibrated and tested in wind tunnel experiments, and from these tests it can be concluded that computational estimates as well as experimental results showed that the developed microsensors function properly and can be a valuable tool in the study of laminar and turbulent flows near a wall. They have reasonably small errors and good frequency response compared to convectional devices. An important finding is that these microsensors do not suffer from the major disadvantages of flush-mounted hot films, however, like all complex tools, they must be used with caution and with an understanding of the phenomena behind their operation.

Acknowledgments

M.S. thanks the Chalmers University of Technology for hosting him during his sabbatical when this work was carried out. Thanks are also due to the Swedish Research Council for financial support. Useful comments by two referees are highly acknowledged as well.

References

Alfredsson, P., Johansson, A., Haritonidis, J. and Eckelmann, H.: 1988, The fluctuating wall-shear stress and the velocity-field in the viscous sublayer, *Phys. Fluids* **31**, 1026–1033.

Bellhouse, B. and Schultz, L.: 1966, Determination of mean and dynamic skin friction separation in low-speed flow with a thin-film heated element, *J. Fluid Mech.* **24**, 379–400.

Bhatia, J., Durst, F. and Jovanovic, J.: 1982, Corrections of hot-wire anemometer measurements near walls, *J. Fluid Mech.* **122**, 411–431.

Blackwelder, R.: 1981, Hot-wire and hot-film anemometers, *in* R. Emrich (ed.), *Methods of Experimental Physics – Fluid Dynamics*, Vol. 18A, Academic Press, pp. 259–314.

Bradshaw: 1971, *An introduction to turbulence and its measurements*, Pergamon Press, Oxford, U.K.

Bruun, H.: 1995, *Hot-wire anemometry*, Oxford University Press, Oxford, New York.

Chew, Y., Khoo, B. and Li, G.: 1994, A time-resolved hot-wire shear-stress probe for turbulent-flow — use of laminar-flow calibration, *Exp. Fluids* **17**, 75–83.

Chew, Y., Khoo, B. and Li, G.: 1998, An investigation of wall effects on hot-wire measurements using a bent sublayer probe, *Meas. Sci. Tech.* **9**, 67–85.

Chew, Y., Khoo, B., Lim, C. and Teo, C.: 1998, Dynamic response of a hot-wire anemometer. Part II: A flash mounted hot-wire and hot-film probes for wall shear stress measurements, *Meas. Sci. Tech.* **9**, 764–778.

Comte-Bellot, G.: 1976, Hot-wire anemometry, *Ann. Rev. Fluid Mech.* **8**, 209–231.

Fernholz, H., Janke, G., Schober, M., Wagner, P. and Warnak, D.: 1996, New developments and applications of skin-friction measuring techniques, *Meas. Sci. Tech.* **7**, 1396–1409.

Haasl, S., Mucha, D., Chernoray, V., Ebefors, T., Enoksson, P., Löfdahl, L. and Stemme, G.: 2002, Hybrid mounted micromachined aluminium hot wire for near wall turbulence measurements, *14th Annual International Conference on Micro Electro Mechanical Systems.*

Hanratty, T. and Campbell, J.: 1996, Measurement of wall-shear stress, *in* R. Goldstein (ed.), *Fluid Mechanics Measurements*, Taylor and Francis, pp. 575–640.

Haritonidis, J.: 1989, The measurements of wall-shear stress, *in* M. Gad-el Hak (ed.), *Advances in Fluid Mechanics Measurements*, Springer-Verlag, pp. 229–261.

Hinze, J.: 1975, *Turbulence*, 2 edn, McGraw-Hill, New York, NY.

Huang, J., Tung, S., Ho, C., Liu, C. and Tai, Y.: 1996, Improved micro thermal shear-stress sensor, *IEEE transactions on instrumentation and measurement* **45**(2), 1–5.

Janke, G.: 1987, Hot wire in wall proximity, *in* G. Comte-Bellot and J. Mathieu (eds), *Advances in Turbulence*, Springer, Berlin, pp. 488–498.

Jiang, F., Tai, Y.-C., Ho, C.-M. and Li, W.: 1994, A micromachined polysilicon hot-wire anemometer, *Solid-State Sensor and actuator Workshop*, Hilton Head.

Kälvesten, E.: 1996, Pressure and wall shear stress sensors for turbulence measurements, *Technical Report TRITA-ILA-9601*, Stockholm, Sweden.

Kälvesten, E., Vieder, C., Löfdahl, L. and Stemme, G.: 1996, An integrated pressure-velocity sensor for correlation measurements in turbulent gas flows, *Sensors Actuators A* **52**, 51–58.

Khoo, B., Chew, Y. and Li, G.: 1996, Time-resolved near-wall hot-wire measurements: use of laminar flow wall correction curve and near-wall calibration technique, *Meas. Sci. Tech.* **7**, 564–575.

Khoo, B., Chew, Y. and Li, G.: 1997, Effects of imperfect spatial resolution on turbulence measurement in the very near-wall viscous sublayer region, *Exp. Fluids* (22), 327–335.

Khoo, B., Chew, Y., Lim, C. and Teo, C.: 1998, Dynamic response of a hot-wire anemometer. Part I: A marginally elevated hot-wire probe for near-wall velocity measurements, *Meas. Sci. Tech.* **9**, 751–763.

Khoo, B., Chew, Y. and Teo, C.: 2000, On near-wall hot-wire measurements, *Exp. Fluids* **29**, 448–460.

Khoo, B., Chew, Y., Teo, C. and Lim, C.: 1999, Dynamic response of a hot-wire anemometer. Part II: Voltage-perturbation versus velocity-perturbation testing for near-wall hot-wire/film probes, *Meas. Sci. Tech.* **10**, 152–169.

Kramers, H.: 1946, Heat transfer from spheres to flowing media, *Physica* **12**, 61–80.

Krishnamoorthy, L., Wood, D., Antonia, R. and Chambers, A.: 1985, Effect of wire diameter and overheat ratio near a conducting wall, *Exp. Fluids* **3**, 121–127.

Lange, C., Durst, F. and Breuer, M.: 1999, Correction of hot-wire measurements in the near-wall region, *Exp. Fluids* (26), 475–477.

Liepmann, H. and Skinner, G.: 1950, Shearing stress measurements by use of a heated element, *Technical Report 1284*, NACA.

Ligrani, P. and Bradshaw, P.: 1987, Spatial resolution and measurement of turbulence in the viscous sublayer using subminiature hot-wire probes, *Exp. Fluids* (5), 407–417.

Löfdahl, L. and Gad-el-Hak, M.: 1999, Mems applications in turbulence and control, *Progr. Aerospace Sci.* **35**(2), 101–195.

Ludwieg, H.: 1950, Instrument for measuring the wall shearing stress of turbulent boundary layers, *Technical memorandum 1284*, NACA, Washington, D.C.

Nagano, Y. and Tsuji, T.: 1994, Recent developments in hot-wire and cold-wire techniques for measurements in turbulent shear flows near walls, *Exp Thermal Fluid Sci* **9**, 94–110.

Österlund, J. and Johansson, A.: 1995, Dynamic behavior of hot-wire probes in turbulent boundary layers, *Advances in turbulence* **5**, 398–402.

Panton, R.: 1996, *Incompressible flow*, John Wiley & Sons, Inc., New York, NY.

Perry, A.: 1982, *Hot-wire anemometry*, Clarendon Press, Oxford, U.K.

Polyakov, A. and Shindin, S.: 1978, Peculiarities of hot-wire measurements of mean velocity and temperature in the wall vicinity, *Lett. Heat and Mass Transfer* **5**, 53–58.

Stein, C., Johansson, P., Bergh, J., Löfdahl, L., Sen, M. and el Hak, M. G.: 2002, An analytical asymptotic solution to a conjugate heat transfer problem, *Int J. Heat Mass Transfer* **45**, 2485–2500.

Teo, C., Khoo, B. and Chew, Y.: 2001, The dynamic response of a hot-wire anemometer: IV. Sine-wave voltage perturbation testing for near-wall hot-wire/film probes and the presence of low-high frequency responce characteristics, *Meas. Sci. Tech.* **12**, 37–51.

Wagner, P.: 1991, The use of near-wall hot-wire probes for time resolved skin-friction measurements, *in* A. Johansson and P. Alfredsson (eds), *Advances in Turbulence*, Vol. 3, Springer-Verlag, pp. 524–529.

Warnack, D.: 1996, *Eine experimentelle Untersuchung beschleunigter turbulent Wandgrenzschichten*, PhD thesis, Technische Universitat Berlin.

Winter, K.: 1977, An outline of the techniques available for the measurement of skin friction in turbulent boundary layers, *Prog. Aerospace Sci.* **18**, 1–55.

Zemskaya, A., Levitskiy, V., Repik, Y. and Sosedko, Y.: 1979, Effect of the proximity of the wall on hot-wire readings in laminar and turbulent boundary layers, *Fluid Mech. — Sov. Res.* **8**, 133–141.